Research Square

Preprints are preliminary reports that have not undergone peer review.
They should not be considered conclusive, used to inform clinical practice,
or referenced by the media as validated information.

Satellite Cell Activation and Altered Cell Cycle Regulation in Beckwith-Wiedemann Syndrome Macroglossia

Katharine Striedinger

kathystriedinger@gmail.com

University of California San Francisco

Jason H Pomerantz

University of California San Francisco

Research Article

Keywords: Beckwith-Wiedemann syndrome, macroglossia, CDKN1C, satellite cells, PAX7, single-cell multiome, CDK inhibitor

Posted Date: November 10th, 2026

DOI: https://doi.org/10.21203/rs.3.rs-11395696/v1

License: This work is licensed under a Creative Commons Attribution 4.0 International License.
Read Full License

Additional Declarations: No competing interests reported.

Abstract

Background

Macroglossia is a cardinal feature of Beckwith-Wiedemann syndrome (BWS), an overgrowth disorder caused by epigenetic changes at 11p15, but its cellular pathogenesis is poorly defined. We investigated whether cell-cycle control in tongue satellite cells and muscle progenitors is altered in BWS and whether cyclin-dependent kinase (CDK) inhibition can modulate their proliferation.

Methods

Human muscle satellite cells (Hu-MuSC) were sorted by flow cytometry from the tongues of children with BWS and from healthy muscle, and their proliferation was measured by EdU incorporation with and without indirubin-3'-monoxime, a CDK and GSK-3β inhibitor. Tongue tissue from children undergoing tongue reduction surgery was analyzed by histology and PAX7/Ki67 immunofluorescence, and satellite cells from one BWS tongue were profiled by single-nucleus multiome sequencing (gene expression and chromatin accessibility) and compared with adult satellite-cell references.

Results

Histology of BWS tongue showed disorganized muscle architecture, variable myofiber size and centrally located nuclei. Ki67 + nuclei were more frequent in two BWS tongues (3.2% and 4.9%) compared to tongue from a child with macroglossia without BWS (1.0%) or adult tongue (0.5%). PAX7 + cells were more frequent in BWS than in adult tongue but similar to non-BWS pediatric macroglossia tongue. The Ki67 + fraction of PAX7 + cells was higher in one of two BWS tongues. BWS satellite cells from one tongue, relative to those from adult skeletal muscle, included more nuclei expressing cell-cycle genes (MKI67 or TOP2A) or MYOG, and their MYOD1, MYOG and SOX8 promoters were more accessible. Within matched cell activation states, CDKN1C was detected less often in BWS satellite cells than in adult muscle. Chromatin at KvDMR1, the imprinting control region of the CDKN1C domain, was more accessible than in adult libraries. In healthy Hu-MuSC, CDKN1C expression decreased upon ex vivo activation. Indirubin-3'-monoxime reduced EdU incorporation in Hu-MuSC from all seven donors, four with BWS and three healthy (Wilcoxon test, P = 0.016).

Conclusions

In BWS tongue satellite cells characteristics of activation and decreased cell-cycle regulation predominate, possibly through reduced CDKN1C-mediated restraint. Indirubin-3'-monoxime reduced their proliferation in vitro, as in non-BWS cells, making CDK or GSK-3β activity a candidate target for further study in macroglossia.

Background

Beckwith-Wiedemann Syndrome (BWS) is a rare genetic disorder that primarily affects growth and development, both before and after birth. Characterized by a wide range of clinical features, the condition commonly includes overgrowth (macrosomia), abdominal wall defects such as omphalocele or umbilical hernia, enlarged tongue (macroglossia), and an increased risk of childhood cancers—especially Wilms tumor and hepatoblastoma [1–4].

BWS is caused by abnormalities in genes located on chromosome 11p15, which are involved in regulating growth. These genetic changes typically affect a process called genomic imprinting, where the expression of certain genes depends on whether they are inherited from the mother or the father [2, 5].

The severity and specific features of BWS can vary widely from one individual to another, making early diagnosis and personalized management crucial. With appropriate medical care and regular screening for complications, many children with Beckwith-Wiedemann Syndrome lead healthy lives.

Macroglossia, or an abnormally large tongue, is one of the most common and recognizable features of Beckwith-Wiedemann Syndrome (BWS), affecting approximately 80% of individuals with the condition [6]. It is caused by overgrowth of muscle and connective tissue in the tongue, which can be present at birth or become more noticeable in early infancy.

In BWS, macroglossia can lead to several complications, including difficulties with feeding, breathing, speech development, and dental alignment. It may also contribute to open bite or mandibular overgrowth due to the constant pressure of the enlarged tongue on developing facial bones. Management of macroglossia depends on its severity. Mild cases may not need intervention; the only treatment for severe cases is tongue reduction surgery (glossectomy) [7, 8], which is painful, associated with a prolonged recovery and can result in functional complications (deformity, altered speech and taste). Furthermore, glossectomy has limited application in posterior and dorsal resections and it is therefore not helpful for treatment of airway obstruction in BWS [9].

While the clinical presentation is well described, the cellular and molecular mechanisms underlying tongue overgrowth remain poorly defined. In this study we aim to understand the causes of macroglossia in BWS and the muscle cell signaling pathways associated with abnormal tongue growth to design better treatments based on a mechanistic rationale.

Macroglossia in Beckwith-Wiedemann Syndrome is primarily the result of dysregulation of imprinted genes on chromosome 11p15.5, a region crucial for controlling growth. This region contains two important domains, each regulated by different imprinting control regions (ICRs): ICR1 (Imprinting Control Region 1) – controls IGF2 and H19 genes and ICR2 (Imprinting Control Region 2) – controls CDKN1C, KCNQ1, and KCNQ1OT1 [1, 10–12].

The dysregulation of imprinted genes leads to overexpression of IGF2 (Insulin-like Growth Factor 2), a paternally expressed gene that promotes cell growth and proliferation [13]. In BWS, gain of methylation at ICR1 or paternal uniparental disomy (pUPD) can lead to biallelic expression of IGF2, causing tissue overgrowth, including in the tongue [12, 14–16]. These lesions can also reduce expression of CDKN1C. CDKN1C is a maternally expressed gene that acts as a cell cycle inhibitor. CDKN1C encodes p57Kip2, a cyclin-dependent kinase inhibitor and negative regulator of fetal growth [17]. In BWS, loss of methylation at ICR2 or mutations in the CDKN1C gene can lead to reduced expression, removing this “growth brake” and contributing to overgrowth of the tongue and other tissues [2, 12].

Macroglossia appears to be less frequent or with less severe morphology in pUPD11 than in IC2 loss of methylation (IC2 LOM) [18].

The tongue is composed largely of skeletal muscle, and both skeletal muscle hyperplasia [19] and myofiber hypertrophy [20] have been reported in BWS macroglossia. Muscle growth, regeneration, and repair in humans depends on skeletal muscle stem cells known as satellite cells (Hu-MuSC) [21]. In macroglossia associated with BWS, emerging evidence suggests that dysregulated satellite cell activity may contribute to skeletal muscle hyperplasia of the tongue [19], alongside the well-known genetic and epigenetic drivers like IGF2 overexpression and CDKN1C downregulation [2, 12].

Methods

Tissue collection and processing

Seven tongue samples were collected from UCSF Craniofacial Center patients who underwent tongue reduction (a 4-year-old male with a clinical diagnosis of BWS; a 7-month-old male with BWS and IC2 LOM; a 4-year-old female with macroglossia due to vascular malformation; an 8-year-old female with macroglossia and a BWS diagnosis; two 10-month-old females with BWS; and a 9-month-old female with BWS). Patients underwent tongue reduction surgery due to complications in breathing, eating, and dental malformation. In addition, two adult tongue samples without BWS were collected: a 59-year-old male, used for histology (Fig. 1), and a 63-year-old male, used for PAX7 and Ki67 quantification (Fig. 2). One temporalis from a 31-year-old female, and temporalis muscle from a 43-year-old female without BWS were collected as well. For Additional file 1: Fig. S1, sections of BWS tongue from a 10-month-old female and of adult vastus lateralis from a 28-year-old male were stained for PAX7 and CDKN1C. Part of the tongue biopsy was cryopreserved for histopathology, and the other part processed for fluorescence activated cell sorting (FACS) to isolate satellite cells according to the procedures described before [22] and continue with downstream applications including multiomics.

Ethics

Human tissue was collected under protocol 11-07323, approved by the Institutional Review Board of the University of California, San Francisco (UCSF). Written informed consent was obtained from all adult

participants and from the parents or legal guardians of minors with their assent when appropriate based on age.

Isolation of Hu-MuSC

We have previously developed methods for isolation and purification functional satellite cells from human muscle tissues [22]. This preparation of purified and minimally altered satellite cells enables in vitro and in vivo experimentation as well as translational applications. Immediately after surgical resection, muscle was stored at 4°C in collection medium (DMEM high glucose with 30% FBS and penicillin–streptomycin). For the activation model, the biopsy was divided 12 h before processing: two-thirds was kept at 4°C as the quiescent sample, and the remaining third was minced immediately with a blade for the activated sample. Single-cell suspensions were obtained by enzymatic dissociation with 1 mg/ml collagenase XI (Sigma-Aldrich) in DMEM with high glucose, 10% FBS and 1% penicillin–streptomycin and filtration, and CD45 + and CD31 + cells were depleted by magnetic-activated cell sorting (MACS LD columns; CD45 and CD31 MicroBeads, Miltenyi Biotec 130-045-801 and 130-091-935). Cells were stained with eFluor 450-conjugated lineage antibodies against CD31, CD34 and CD45 (eBioscience 48-0319-42, 48-0349-42 and 48-0459-42), CD56 APC-Vio770 (Miltenyi Biotec 130-100-694) and antibodies against CD29 and CXCR4 (eBioscience), and dead cells were excluded with SYTOX Blue (1:1000). To specifically sort Hu-MuSC, we used the same gate (P5) for all BWS and control samples, selecting lineage-negative CXCR4 + CD29+ CD56 + cells, as described in our previous studies [23–25] and in our detailed published protocol [22]. For the activated sample, the minced tissue was incubated for 12 h at 37°C in 30 ml of growth medium (Ham's F10, 20% FBS, penicillin–streptomycin, 2 mM HEPES and 5 ng/ml FGF2) in a low-attachment plate, then collected, washed in PBS, centrifuged at 2,000 rpm for 5 min, and digested and stained together with the quiescent sample from the same donor [22]. Samples were collected and accessed for research purposes between 2016 and 2023.

Hu-MuSC culture and EdU proliferation assay

Hu-MuSC isolated as described above [22, 24] were plated at 10,000 cells per well in Matrigel-coated 48-well plates in growth medium (DMEM with 20% FBS) and cultured at 37°C in 5% CO_2. Proliferation was measured by EdU incorporation using the Click-iT EdU Alexa Fluor 488 Imaging Kit (Thermo Fisher Scientific, C10337), as in our previous study [26]. EdU was added to the medium at 1:1000 (2 µL of a 10 mM stock per 2 mL; final concentration 10 µM) together with the treatments on day 0, and cells were fixed in 10% neutral-buffered formalin for 15 min at room temperature on day 3, washed twice in 3% BSA in PBS, permeabilized with 0.5% Triton X-100 in PBS, blocked in 3% BSA in PBS, and incubated with the Click-iT reaction cocktail (240 µL per well) for 30 min at room temperature in the dark (adapted from [27]). Nuclei were stained with Hoechst 33342 (1:2000 in PBS, 30 min at room temperature) and imaged. Cells were then blocked for 1 h in 10% normal horse serum and immunostained overnight for MYOD (mouse monoclonal, BD Pharmingen, 554130; 1:100) followed by an Alexa Fluor 594 anti-mouse secondary antibody (1:1000). Images were acquired on a Leica DMI8 (AF6000) widefield microscope

with a 10× objective as tiled images of each well. EdU+ nuclei were then counted on 15 fields per donor and condition imaged at 63× on an inverted Zeiss LSM900 laser scanning confocal microscope and expressed as a percentage of all Hoechst+ nuclei.

Indirubin-3'-monoxime and myostatin treatment

Hu-MuSC were treated from day 0 to day 3 with the CDK/GSK-3β inhibitor indirubin-3'-monoxime (Abcam, ab141296) at a final concentration of 5 µM (1 µL of a 10 mM stock in DMSO per 2 mL of medium) or with recombinant human myostatin (GDF-8; R&D Systems, 788-G8) at 1 µg/mL. Vehicle-treated cells (0.05% DMSO) served as controls. Myostatin was reconstituted at 100 µg/mL in 4 mM HCl containing 0.1% BSA. Concentrations were chosen based on published activity of the inhibitor [28, 29] and on myostatin effects in human myoblasts [30]. Healthy Hu-MuSC from three donors (14, 15 and 44 years old) and BWS Hu-MuSC from four patients (4 years, 7 months, 9 months and 10 months old) were tested.

siRNA knockdown of CDKN1C

Hu-MuSC were transfected with 10 or 40 pmol of siRNA targeting CDKN1C (Silencer Select, Ambion, 4390824; siRNA ID s2841) or a non-targeting scrambled control siRNA, in parallel wells of the same cells from the same donor (paired, donor-matched design), using Lipofectamine RNAiMAX in Opti-MEM according to the manufacturer's instructions. Cells were transfected on day 1, the medium was replaced 24 h later, and cells were fixed or harvested on day 3. Knockdown was confirmed by RT-qPCR on day 3 (CDKN1C 0 to 0.36 of control across five measurements from three donors (14, 15 and 44 years; the same donors as the paired EdU experiment); about 86% knockdown), and proliferation was assessed by EdU incorporation as above. The approach was adapted from knockdown of p57 in primary human myoblasts [31] and in muscle cells [32].

Images were acquired on a Leica DMi8 inverted widefield fluorescence microscope with a Leica DFC9000 GT sCMOS camera and LAS X software (v3.7.1; Leica Microsystems), using a 40×/0.60 HC PL FLUOTAR L objective.

Histology and immunohistochemistry

OCT-embedded tongue specimens were obtained from patients undergoing tongue reduction surgery and from the adult tongues listed above. All human tissue collection followed protocols approved by the institutional review board (IRB).

Sections were cut on a cryostat at 10 µm for H&E and 6 µm for immunofluorescence and mounted on Superfrost™ Plus adhesive glass slides (Thermo Fisher Scientific).

Hematoxylin and eosin (H&E) staining

Cryopreserved tongue specimens were sectioned at 10 µm thickness and mounted on Superfrost™ Plus glass slides (Thermo Fisher Scientific). Sections were air-dried, fixed in 10% neutral buffered formalin for 10 min, and rinsed in distilled water. Sections were stained with Gill's hematoxylin for 4 minutes, rinsed in tap water, blued in Scott's tap water for 3 minutes, rinsed, counterstained with eosin for 2 minutes, rinsed, dehydrated through graded ethanol (80%, 95% and 100%), cleared in xylene and mounted with Permount.

Histological evaluation was conducted under brightfield microscopy (Leica) at 10×, 20×, and 40× magnification. Tongue muscle was assessed for myofiber architecture and size, central nuclei and inflammatory infiltrates.

Images were acquired using a microscope-mounted digital camera.

Immunohistochemistry (IHC)

Antigen retrieval and blocking

Adjacent cryosections were fixed in 4% PFA. Non-specific binding was minimized using 2% normal goat serum (Vector Laboratories) in PBS for 30 minutes at room temperature. The following primary antibodies were used:

For PAX7 detection, permeabilization in 0.1% Triton X-100 was performed, followed by immunostaining:

- Mouse anti-PAX7 (1:10; DSHB, clone PAX7) — satellite-cell marker
- Rabbit anti-Ki67 (1:200; Abcam, ab16667)
- Anti-p57KIP2/CDKN1C (Santa Cruz Biotechnology, sc-56341; mouse monoclonal IgG2b; 1:200) for Additional file 1: Fig. S1
- Human spectrin (Leica Microsystems, NCL-SPEC1; 1:100; same antibody as in Garcia et al. [23, 24]) to outline myofibers; the sections for Fig. 2 were also stained with rat anti-laminin (Sigma-Aldrich, L0663; 1:500) to outline the basal lamina

Primary antibodies were incubated overnight at 4°C in a humidified chamber.

After rinsing in PBS, sections were incubated with fluorescent secondary antibodies, goat anti-mouse Alexa Fluor 594 (Thermo Fisher Scientific; 1:250; PAX7 is shown in magenta in all figures except Additional file 1c, where laminin is magenta and PAX7 is shown in white) for PAX7 and goat anti-rabbit Alexa Fluor 488 for Ki67 (Thermo Fisher Scientific; 1:250) for 30 minutes at room temperature. Slides were counterstained with DAPI (1 µg/mL) for nuclear visualization and coverslipped with ProLong™ Gold Antifade Mountant (Thermo Fisher).

Negative and Positive Controls: Negative controls were performed by omitting the primary antibody.

Positive control tissues (e.g., normal skeletal muscle) were used to confirm antibody performance.

PAX7+, Ki67 + and PAX7 + Ki67+ nuclei were counted manually on 13 to 35 fields per tongue imaged at 63× on an inverted Zeiss LSM900 laser scanning confocal microscope and pooled per tongue. Two imaged fields from the 10-month-old BWS tongue lacked complete counts (one was not scored for PAX7 or Ki67, and one had no nucleus count) and were excluded from that tongue's totals. For display, all adjustments were linear and applied to whole images or whole channels: H&E images were white-balanced with one gain per colour channel (at most 6.3%; one image without blank background was not adjusted), and immunofluorescence images were brightened with one gain per image or one linear contrast stretch per channel; no local edits were made. Satellite cells were identified by PAX7 + nuclei located adjacent to myofibers, at the spectrin-outlined sarcolemma. PAX7 + Ki67+ nuclei were assessed similarly. PAX7 + and Ki67 + nuclei were expressed as a percentage of all DAPI+ nuclei, and PAX7 + Ki67+ nuclei as a percentage of PAX7 + nuclei.

Satellite cells were defined as PAX7 + DAPI+ nuclei; human spectrin outlined the myofibers. The percentage of PAX7 + cells that were Ki67 + was also calculated [33].

Statistical analysis was performed using GraphPad Prism (v10.0). EdU incorporation with and without indirubin-3'-monoxime was compared across donors with an exact two-sided Wilcoxon signed-rank test, baseline EdU in BWS and non-BWS cells with an exact Mann–Whitney test, each treatment in the screen with its control across the three matched non-BWS donors with a two-sided paired t-test, without correction for multiple comparisons, and CDKN1C RT-qPCR values in control and activated cells with an exact two-sided Wilcoxon signed-rank test; $p < 0.05$ was considered significant. Tissue PAX7 and Ki67 counts were not tested statistically, because each group contained one or two tongues.

Single-cell assay for transposase-accessible chromatin (scATAC) in human satellite cells

All protocols to generate scATAC-seq data using the 10x Chromium platform, including sample preparation, library preparation and instrument and sequencing settings, are described below and are also available here: https://support.10xgenomics.com/single-cell-atac.

To investigate the differentially open chromatin regions in close-to-quiescence (control) vs. activated Hu-MuSC after the overnight activation model, right after the FACS isolation, the nuclei were isolated following guidelines for limited number and fragile cells by 10x Demonstrated protocol (Nuclei Isolation for Single Cell ATAC Sequencing CG000169 Rev E) and the nuclei sample from close-to-quiescence and activated Hu-MuSC were loaded into the chromium chip by the UCSF Genomic core for scATAC. The close-to-quiescence and activated libraries came from a vastus lateralis biopsy from a 56-year-old male and were previously published by our laboratory [26]; the data and analysis scripts are available at github.com/kstriedinger/PomerantzLab_ATAC1. For CDKN1C expression in the activation model,

quiescent and activated Hu-MuSC from six independent healthy donors (donor-matched control and activated) were analysed by RT-qPCR (RNA isolated with the RNeasy kit, Qiagen 74104, with on-column DNase digestion, Qiagen 79254; reverse transcription with the High-Capacity cDNA Reverse Transcription kit, Thermo Fisher Scientific 4368814; pre-amplification for 18 cycles with PreAmp Master Mix, Fluidigm 100-5876C2, with products diluted 1:10; TaqMan Universal Master Mix II, with UNG, Thermo Fisher Scientific 4440038, 20 µL reactions in triplicate, on a ViiA 7 real-time PCR system (Life Technologies), as in our previous study [26]; CDKN1C TaqMan assay Hs00175938_m1; normalized to ACTB (Hs99999903_m1) or GAPDH (Hs02758991_g1)). Relative expression was calculated as 2^−ΔCt against the reference gene, without a calibrator sample. Control and activated values were compared with an exact two-sided Wilcoxon signed-rank test (n = 6 donor-matched pairs), used because the activated values included non-detects.

The scATAC-seq libraries were prepared and sequenced according to the Chromium Single Cell ATAC Reagent Kits User Guide (10x Genomics; CG000168 Rev B) and the BCL files subjected to the Cell Ranger pipeline. (Cell Ranger Software v.1.2.0; https://support.10xgenomics.com/single-cell-atac/software/pipelines/latest/algorithms/overview).

Data processing using Cell Ranger ATAC software 1.2.0 (https://support.10xgenomics.com/single-cell-atac/software/pipelines/latest/what-is-cell-ranger-atac) and Loupe Cell Browser Version 5.0.1 (https://support.10xgenomics.com/single-cell-atac/software/visualization/latest/what-is-loupe-cell-browser) were used as described before [34].

Analysis was performed in R [35] with Seurat v4.3.0 [36] and Signac v1.9.0 [37, 38] as described [26]. Nuclei were retained with 3,000–20,000 fragments in peaks, > 15% of reads in peaks, a blacklist ratio < 0.05, a nucleosome signal < 4 and a TSS enrichment score > 2; data were normalized by TF-IDF, reduced by singular value decomposition (latent semantic indexing), and LSI components 2–30 were used for UMAP and graph-based clustering.

Transcription factor motif activity was estimated per cell with chromVAR [39] using JASPAR motifs MA0680.1, MA0868.2, MA0499.2, MA0476.1 and MA0500.2, shown alongside PAX7, SOX8, MYOD1, FOS and MYOG expression.

Single-cell multiome (scRNA-seq + ATAC-seq)

Nuclei were isolated immediately after FACS, without culture, to preserve most of the sorted cells and their genomic signature. For FACS-purified Hu-MuSC, nuclei were isolated from 40,000 of 51,635 sorted cells following the 10x Genomics Demonstrated Protocol for low cell input (CG000365) [40], with lysis buffer (10 mM Tris-HCl pH 7.4, 10 mM NaCl, 3 mM MgCl2, 0.1% Tween-20, 0.1% Nonidet P-40, 0.01% digitonin, 1% BSA, 1 mM DTT and 1 U/µL RNase inhibitor) for 4 min on ice, passed through a 40 µm Flowmi cell strainer, counted with trypan blue on a Countess cell counter (about 4,000–5,000 nuclei/µL), and loaded onto the Chromium chip targeting about 3,000 nuclei. Quality-control thresholds and

annotation of muscle stem cell clusters followed recent human skeletal muscle multiome studies [41, 42].

Library preparation and sequencing

Single-cell ATAC and gene expression libraries were generated using the Chromium Next GEM Single Cell Multiome ATAC + Gene Expression kit (10x Genomics, PN-1000283), following the manufacturer's instructions.

- Transposition: Nuclei were tagmented with Tn5 transposase to fragment open chromatin.
- Barcoding and Reverse Transcription: Nuclei were encapsulated in Gel Bead-In-Emulsion (GEMs), enabling simultaneous reverse transcription of mRNA and tagging of accessible chromatin.
- Library Construction: ATAC and cDNA libraries were amplified separately and purified using SPRIselect beads.

Libraries were quantified by Qubit fluorometry and Bioanalyzer (Agilent) and sequenced on an Illumina NovaSeq 6000 with the following read configuration:

- Gene Expression: 28 bp (Read 1) + 90 bp (Read 2)
- ATAC: 50 bp paired-end

Data processing and quality control

Raw FASTQ files generated from the Chromium Single Cell Multiome platform (10x Genomics) were aligned and processed using Cell Ranger ARC (v2.0.1) with the GRCh38 human reference genome provided by 10x Genomics. Cell Ranger ARC called 2,914 nuclei, with medians of 14,424 high-quality ATAC fragments and 852 genes per nucleus, from 365,767,238 gene-expression read pairs. This pipeline simultaneously performed:

- Read alignment via STAR (RNA) and BWA (ATAC)
- Barcode demultiplexing
- UMI counting (RNA)
- Peak calling (ATAC) using MACS2
- Initial cell calling and gene-barcode matrices output

Data integration and analysis (Seurat + Signac)

All downstream analysis was performed in R (v4.3.1) using the Seurat (v5.0.1) and Signac (v1.12.0) packages.

- Gene expression was normalized using SCTransform [43].
- ATAC-seq peaks were quantified and linked to nearby genes.

- Dimensionality reduction was performed using weighted nearest neighbors (WNN) for multimodal integration.
- Cell clusters were identified by shared nearest neighbor (SNN) graph clustering and annotated based on marker genes.

Comparison with adult satellite-cell reference data

Single-cell transcriptomes of FACS-purified satellite cells from limb and trunk muscles of 12 healthy adult donors aged 20 to 87 years (Chromium Single Cell 3' v3, 10x Genomics), previously published by our laboratory [25] (Dryad, doi:10.7272/Q65X273X), were used as a reference for the BWS multiome. The adult references used here, this scRNA-seq set and the close-to-quiescence and activated scATAC libraries of the 56-year-old male described below [26], are previously published datasets from our laboratory; the 52-year-old male scATAC library described below is new to this study. BWS nuclei with at least 500 detected genes, less than 20% mitochondrial reads and at least 1,000 non-mitochondrial UMIs (required for down-sampling to 1,000 UMIs), and adult cells with at least 500 genes and less than 15% mitochondrial reads, were retained. Myogenic cells were defined as those in which myogenic markers (PAX7, MYF5, CDH15, DES, MYOD1, MYOG, CHRNA1 and APOE) outnumbered fibroblast markers, giving 821 BWS nuclei and 609 to 19,140 cells per adult donor. Genes were matched on Ensembl identifiers (32,290 shared genes), mitochondrial genes were excluded, and every cell was down-sampled to 1,000 UMIs. Each cell was assigned to one class, in this order: cycling (MKI67 or TOP2A detected), MYOG+, MYOD1+ (without MYOG), and PAX7 + without MYOD1 or MYOG (quiescent-like); this one-class assignment was used for the within-state CDKN1C comparison. The state fractions reported in Results skip the cycling step, so a cycling cell is also counted under its PAX7, MYOD1 or MYOG state. A gene was counted as detected when at least one UMI remained after down-sampling (fixed random seed). The percentage of myogenic cells in each class and the percentage detecting selected genes were calculated per donor; for CDKN1C detection within each class, donor–class groups with fewer than 20 cells were excluded.

For chromatin, ATAC fragments from the same 821 BWS nuclei and from three adult Hu-MuSC scATAC libraries from two healthy donors (one previously unpublished close-to-quiescence library, deposited with this study, from freshly purified vastus lateralis satellite cells of a 52-year-old male (FACS-sorted lineage-negative CD56 + CD29+ CXCR4 + cells, without the overnight activation step; 10x Genomics Single Cell ATAC v1 chemistry), 1,200 nuclei, sequenced at the UCSF core, on the same sequencer as our earlier study [25] and in the same 2020 run as the 56-year-old male libraries and processed with Cell Ranger ATAC 1.2 (GRCh38), who is also one of the 12 adult scRNA-seq donors [25]; and, from a 56-year-old male, a close-to-quiescence library of freshly purified satellite cells and a matched activated library, prepared with the purification and activation protocols of our previous study; both were published in that study [26]) were counted at each gene promoter (TSS ± 1 kb) and at KvDMR1 (chr11:2,697,900–2,701,500, GRCh38) and normalized to the total promoter fragments of each library. BWS/adult log2 ratios were ranked against all 19,998 promoters with at least 50 fragments. Because there was a single

BWS donor, comparisons with adult donors were descriptive and were not tested statistically. Coverage tracks are shown on GRCh38 (hg38) for the close-to-quiescence and activated scATAC libraries of the 56-year-old male and for the multiome with all three adult libraries.

Results

Histological analysis reveals disorganized muscle architecture in BWS macroglossia

H&E-stained tongue sections from BWS patients exhibited highly densely packed muscle fibers, disorganized muscle architecture and variable size of myofibers. There was frequent presence of centrally located nuclei, indicative of regeneration or immature muscle. In contrast, control samples displayed regularly spaced myofibers with peripherally located nuclei. No inflammatory infiltrates were noted in either group (Fig. 1).

PAX7 + and Ki67 + cells are more frequent in BWS macroglossia

In tongue sections, PAX7 + nuclei comprised 12.3% and 16.6% of all nuclei in the two BWS tongues (7 months and 10 months; 754 and 446 nuclei counted), compared with 10.5% in macroglossia without BWS (4 years; 523 nuclei) and 2.3% in adult tongue (63 years; 561 nuclei). Ki67 + nuclei comprised 3.2% and 4.9% of nuclei in BWS tongue, compared with 1.0% and 0.5% in the non-BWS pediatric and adult tongues. The fraction of PAX7 + cells that were Ki67 + was 18.3% (17/93) and 8.1% (6/74) in the two BWS tongues, compared with 5.5% (3/55) in macroglossia without BWS and 7.7% (1/13) in adult tongue (Fig. 2), so this fraction was not consistently higher in BWS tongue. Pooled across the two BWS tongues, PAX7 + cells made up 13.9% of nuclei (167/1,200) and Ki67 + nuclei 3.8% (46/1,200), and 13.8% of PAX7 + cells were Ki67+ (23/167). Because each group contained one or two tongues, these results are descriptive and were not tested statistically. BWS tongue from another 10-month-old girl also contained many PAX7 + cells, clustered between myofibers, whereas few were seen in adult vastus lateralis from a 28-year-old male (Additional file 1: Fig. S1a, b).

Additional file 1: Figure S1. PAX7 + cells in BWS tongue and in adult limb muscle. (a, b) Immunofluorescence for PAX7 (magenta), CDKN1C (green, antibody) and human spectrin (far red, shown in white) with DAPI (blue); 40× objective (Leica). (a) Adult vastus lateralis from a 28-year-old male. (b) BWS tongue from a 10-month-old female. In (b), many PAX7 + cells lie in clusters between myofibers rather than beneath the basal lamina, so they are described as PAX7 + cells rather than satellite cells; few PAX7 + cells are seen in (a). In (a, b) most CDKN1C signal lies outside PAX7 + cells. Panels a and b are illustrative and were not quantified; the tongue in (b) is not in the Fig. 2 counts, and the samples differ in age and muscle. (c) The 10-month-old female tongue counted in Fig. 2, stained for Ki67 (green), laminin (magenta) and PAX7 (single-channel view only) with DAPI (blue); one tile scan,

Leica HC PL FLUOTAR 20×/0.40 objective. Left, overview; dashed box, area enlarged in the middle. Green arrowhead, Ki67 + nuclei in the basal layer of the surface epithelium (internal positive control). Middle, raw channels; yellow arrow, a PAX7 + Ki67+ nucleus at the edge of a myofiber beneath the laminin-stained basal lamina. Right, that nucleus as separate PAX7 (white), Ki67 (green) and DAPI (blue) channels; a single example cell, not quantified. Scale bars: a, b, 10 µm; c, 500 µm (left), 100 µm (middle) and 10 µm (single channels). File format: TIFF.

PAX7 + cells were localized along the periphery of muscle fibers, consistent with satellite cell identity (Fig. 2).

CDKN1C is downregulated with activation of healthy Hu-MuSC, and multiome profiling of BWS satellite cells

In healthy adult Hu-MuSC, ex vivo activation was accompanied by loss of CDKN1C transcripts, which fell below detection in all six donor-matched pairs (Fig. 3a; exact two-sided Wilcoxon signed-rank test, P = 0.031, n = 6). For context, Fig. 3b, c show chromatin accessibility (scATAC-seq) at the CDKN1C and IGF2 loci in close-to-quiescence (freshly purified) and activated Hu-MuSC of one 56-year-old male, prepared with the activation model of our previous study [26], shown descriptively without statistical comparison. These data are consistent with CDKN1C contributing to the regulation of human satellite-cell activation.

We performed multiome analysis of BWS tongue to gain insight into the molecular underpinnings of BWS in Hu-MuSC. Tongue tissue from an 8-year-old patient with BWS and macroglossia was obtained from tongue reduction surgery. Human satellite cells were isolated and purified using FACS; Cell Ranger ARC called 2,914 nuclei, of which 1,110 passed quality control and 821 were classified as myogenic (see below), and were analyzed using Multiome for both gene expression and DNA accessibility (scRNA and scATAC respectively) in the same cell, we studied the open chromatin regions, gene expression and cellular pathways differentially expressed in satellite cells (Fig. 4).

More BWS satellite cells express cell-cycle and differentiation genes than adult satellite cells

To place the BWS multiome in context, we compared myogenic nuclei with single-cell transcriptomes of FACS-purified satellite cells from limb and trunk muscles of 12 healthy adult donors aged 20 to 87 years, previously published by our laboratory [25]. Every cell was down-sampled to 1,000 UMIs so that detection rates were comparable. Of 821 BWS satellite cells (myogenic nuclei), 7.7% expressed MYOG and 2.1% expressed MKI67 or TOP2A, compared with 0.1–3.8% and 0–1.1% of adult satellite cells. Both fractions were higher than in any adult donor, including the two youngest (20 and 21 years) (Additional file 2: Fig. S2). The fraction of MYOD1 + cells (3.5%) was within the adult range (0.2–3.9%). PAX7 + cells without MYOD1 or MYOG made up 60.3% of BWS myogenic nuclei and 22.6–45.5% of adult satellite cells. Since PAX7 is a long gene that is detected more readily in nuclei than in whole cells we interpreted single-gene differences only when they survived ranking against genes of similar length. Long, nuclear-retained

transcripts such as PAX7 and KCNQ1OT1 were detected more often in BWS satellite cells, and short or immediate-early transcripts such as CDKN1C, FOS and JUNB less often (Additional file 3: Fig. S3). CDK8 was detected in 39.2% of BWS satellite cells against 3.4 to 10.5% across adult donors, a difference that survives ranking against genes of similar length, but its promoter accessibility did not differ from adult libraries (see below) and CDK8 was not tested functionally.

Additional file 2: Figure S2. Cell states in BWS satellite cells compared with adult satellite cells. Percentage of myogenic cells that are PAX7 + without MYOD1 or MYOG, MYOD1+ (activated), MYOG+ (differentiating) or cycling (MKI67 or TOP2A detected), after down-sampling every cell to 1,000 UMIs. Blue circles, FACS-purified satellite cells from 12 healthy adult donors (scRNA-seq), plotted by donor age; orange triangles, BWS satellite cells, myogenic nuclei from the 8-year-old donor (snRNA-seq from the multiome; 821 nuclei). File format: TIFF.

Additional file 3: Figure S3. Detection of selected genes in BWS satellite cells and adult satellite cells. Percentage of myogenic cells in which each of 12 genes (CDKN1C, KCNQ1OT1, IGF2, MKI67, MYOD1, MYOG, PAX7, CDK8, SOX8, HEY1, FOS and JUNB) was detected after down-sampling to 1,000 UMIs. Blue circles, FACS-purified satellite cells from 12 healthy adult donors (scRNA-seq), plotted by donor age; orange triangles, BWS satellite cells (8-year-old female; myogenic nuclei from the multiome). Long and nuclear-retained transcripts (for example PAX7 and KCNQ1OT1) are detected more often in nuclei, and short, cytoplasmic and immediate-early transcripts (for example CDKN1C, FOS and JUNB) less often, so single-gene differences between BWS satellite cells and adult cells were interpreted only when they held after ranking against genes of similar length [75]. File format: TIFF.

CDKN1C is detected less often in BWS satellite cells within matched cell states

Because CDKN1C falls when satellite cells are activated (Fig. 3a), a larger activated fraction alone could lower its detection, so we compared CDKN1C within each cell state. CDKN1C was detected in 5.3% of quiescent-like (PAX7+, MYOD1−, MYOG−) BWS satellite cells (n = 490 nuclei), against a median of 47.2% across the 12 adult donors (range 23.6 to 80.1%); in 0% of MYOD1 + BWS satellite cells, against an adult median of 35.4%; and in 3.2% of MYOG + BWS satellite cells, against 57.2%. In each state the BWS value was below every adult donor with at least 20 cells in that state (Fig. 4c). CDKN1C is a short transcript, which single-nucleus profiling detects less readily, but ranked against the 500 expressed genes closest to it in length, or against genes of similar expression, it remained in the lowest percentiles. Two other cell-cycle regulators, CDKN1B and YAP1, showed no comparable deficit. These data come from a single multiome donor and are descriptive. The related observations of more Ki67 + nuclei in tissue and higher baseline EdU incorporation come from different patients (two and four BWS donors, respectively), among six BWS tongues banked at UCSF between 2016 and 2023 by different researchers for other purposes, not for this study.

KvDMR1 is more accessible in BWS satellite cells than in adult libraries

We next compared promoter chromatin accessibility in the same 821 BWS satellite cells (myogenic nuclei) with three scATAC libraries from healthy adult Hu-MuSC of two donors: a close-to-quiescence library from a 52-year-old male (vastus lateralis; 1,200 nuclei), and the close-to-quiescence and activated libraries of the activation model from a 56-year-old male (Fig. 3), previously published by our laboratory [26]. The BWS multiome and the close-to-quiescence and activated adult libraries are all single-nuclei preparations, so no difference in preparation arises in this comparison. Accessibility at KvDMR1, the IC2 imprinting control region that contains the KCNQ1OT1 promoter, was 1.8- to 1.9-fold higher in BWS than in each adult library (log2 ratios 0.85–0.91), placing it in the top 3–4% of 19,998 promoters (Additional file 4: Fig. S4). In normal cells only the paternal KvDMR1 allele is unmethylated and open, whereas with IC2 loss of methylation or paternal uniparental disomy of 11p15 (pUPD11) both alleles are open. The result is therefore consistent with either lesion in the donor's satellite cells. This patient did not have genetic testing, but IC2 hypomethylation with normal IC1 methylation was confirmed clinically in another patient in this study (the 7-month-old male). The MYOG (log2 ratios 1.67–2.28) and MYOD1 (0.60–1.70) promoters were also more accessible, consistent with the larger fraction of committed and differentiating cells, as was SOX8 (0.44–1.20). Accessibility at the CDKN1C and CDK8 promoters did not differ from the adult libraries (Additional file 4: Fig. S4b–d), so in this donor the lower CDKN1C RNA is not explained by a closed CDKN1C promoter; IC1 and H19 had too few fragments to assess.

Additional file 4: Figure S4. Promoter chromatin accessibility in BWS satellite cells compared with adult Hu-MuSC. (a) Histograms show log2 accessibility ratios (BWS/adult, each normalized to all promoter fragments) for 19,998 promoters (TSS ± 1 kb) with at least 50 fragments, against each of three adult scATAC libraries (52-year-old male, freshly purified and close to quiescence; 56-year-old male, freshly purified and close to quiescence; the same 56-year-old donor, activated [26]). The vertical line marks KvDMR1 (IC2; chr11:2,697,900–2,701,500, GRCh38). (b–d) Chromatin accessibility in BWS satellite cells (8-year-old female; vermillion) and in the same three adult libraries (close to quiescence, light green (52 years) and dark green (56 years); activated, red; in the order of a) across the region from KvDMR1 to CDKN1C (b; grey band, KvDMR1), and enlarged at KvDMR1 (c) and at CDKN1C (d), shown as Tn5 insertions per million promoter fragments on GRCh38 (hg38). CDKN1C promoter accessibility did not differ. File format: TIFF.

Indirubin-3'-monoxime decreases proliferation of healthy and BWS Hu-MuSC

We tested whether the CDK/GSK-3β inhibitor indirubin-3'-monoxime or myostatin altered the proliferation of BWS Hu-MuSC in vitro. EdU uptake by myostatin- and indirubin-3'-monoxime-treated Hu-MuSC from BWS patients and healthy controls was quantified to assess proliferation. Under control conditions, the percentage of EdU+ cells was higher in each of four BWS donors (6.8 to 18.0%; mean 10.7%) than in each of three non-BWS donors (4.5 to 5.5%; mean 5.0%), with no overlap between the groups (exact two-

sided Mann–Whitney test, P = 0.057; Fig. 5a). The BWS donors included the 7-month-old with confirmed IC2 LOM (6.8%) and a 9-month-old (9.6%). Higher baseline proliferation in BWS satellite cells is consistent with the more frequent Ki67 + nuclei in BWS tongue sections and the larger cycling fraction in the BWS multiome, but the donors also differed in age and the groups were small, so we report this comparison descriptively. In non-BWS Hu-MuSC, indirubin-3'-monoxime (5 μM) reduced the percentage of EdU+ cells, whereas recombinant human myostatin (1 μg/mL) and siRNA against CDKN1C (10 pmol) did not reduce it to a similar extent (Fig. 5b). Indirubin-3'-monoxime reduced EdU incorporation in Hu-MuSC from each of three healthy donors (14, 15 and 44 years old) and four patients with BWS (4 years, 7 months, 9 months and 10 months old); the paired difference across the seven donors was significant (exact two-sided Wilcoxon signed-rank test, P = 0.016; Fig. 5c).

Discussion

The observations in this study of Ki67 positivity, increased cell cycle and myogenic gene expression, and KvDMR1 accessibility provide evidence of altered cell-cycle regulation favoring proliferation in BWS satellite cells and early muscle progenitors.

The degree to which reduced CDKN1C directly influences BWS Hu-MuSC proliferation was not directly tested but circumstantial evidence is suggestive. In healthy adult Hu-MuSC, CDKN1C expression fell upon activation (Fig. 3a), consistent with a role for CDKN1C in satellite-cell quiescence, and with single-cell data in which CDKN1C is enriched in quiescent rather than early-activated human satellite cells [44]. In mouse satellite cells, the subcellular localization of Cdkn1c controls growth arrest [27], DNA methylation regulates proliferation through p57Kip2 [45], and quiescent satellite cells are enriched for negative regulators of the cell cycle and myogenic inhibitors [46].

Hyperplasia or hypertrophy. The cellular basis of macroglossia in BWS has been studied in very few patients because of the rarity of the condition. A single-patient histological report described skeletal muscle hyperplasia [19], whereas the largest series to date, 35 tongues from children with IC2 LOM (n = 25) or paternal uniparental disomy of 11p15 (pUPD11, n = 10) compared with six pediatric autopsy tongues, found enlarged myofiber cross-sectional area in both subtypes and concluded that the overgrowth is due to fiber hypertrophy rather than increased fiber number [20]. The histological analysis in our study, which shows densely packed fibers of variable size with frequent central nuclei (Fig. 1), is compatible with either interpretation. The two models are also not mutually exclusive. In postnatal muscle, fiber growth depends first on the addition of myonuclei from proliferating satellite cells and muscle progenitors, and only later on growth of existing fibers [47, 48], so increase in satellite-cell proliferation would be expected to result in larger, more nucleated fibers rather than as more fibers. The central nuclei we observed are consistent with ongoing myonuclear addition or regeneration.

Satellite-cell number and proliferation. In tissue sections, Ki67 + nuclei were more frequent in the two BWS tongues than in macroglossia without BWS or in adult tongue, and PAX7 + cells more frequent than in adult tongue, but the fraction of PAX7 + cells that were Ki67 + was not consistently higher. Normal

postnatal development explains much of the difference from adult tongue. In mouse limb muscle, about 65% of PAX7 + cells are cycling at birth, 29% at four weeks and almost none by eight weeks, when the quiescent pool is established [47]. In human muscle, satellite-cell number per fiber changes little from birth to adulthood while fiber size increases greatly [49], so satellite cells become sparser per unit area as children grow. A comparison of infant BWS tongue with adult tongue therefore mixes BWS with age, and the comparison with pediatric non-BWS macroglossia is the more informative one. For satellite-cell-specific cycling, that comparison is not consistent across our two BWS tongues, which agrees with Tichy et al. [20]. They found similar numbers of PAX7 + cells and no significant difference in satellite-cell Ki67 between BWS tongues and pediatric autopsy controls younger than 3 years, and comparable proliferation of BWS and control satellite cells in growth conditions in vitro. Many Ki67 + nuclei in BWS tongue were PAX7-negative (most of them in one tongue). These may be committed myogenic progenitors that have downregulated PAX7. Our single-nucleus data fit this interpretation, with more nuclei expressing cell-cycle genes or MYOG in the BWS donor than in any adult donor, and more accessible MYOD1, MYOG and SOX8 promoters. In a human muscle atlas that included satellite cells from children aged 7 to 11 years, postnatal satellite cells showed almost no expression of cell-cycle-promoting genes [50]; that study pooled children with adults, so it does not provide an age-matched comparison. Because the donor was 8 years old and the youngest adult 20, part of this difference may still reflect age. The combination of more cell-cycle gene expression with more MYOG+ cells resembles the sustained proliferation during differentiation that Tichy et al. described in IC2 LOM cultures, which was accompanied by enrichment of CDK4/CDK6 activity. pUPD11 cells in the same study instead showed reduced proliferation and activated NOTCH signaling, so pooling subtypes, or comparing a few patients of different subtypes, could mask a subtype-specific increase. Taken together, BWS tongue contains more Ki67 + nuclei overall, and in the multiome donor a larger committed myogenic fraction; these data do not show that a larger fraction of satellite cells is cycling. Whether PAX7 + satellite cells themselves cycle more than expected for age has not yet been shown in tissue.

CDKN1C and cell-cycle control. Reduced CDKN1C is a plausible link between the 11p15 defect and the cell-cycle changes in BWS satellite cells, but with available data including this study, it remains unproven. CDKN1C (p57Kip2) and p21 are together required for cell-cycle exit at the myogenin step of differentiation [51], and CDKN1C inhibits cyclin E–CDK2 in proliferating myoblasts [52]. Genetic evidence that loss of p57Kip2 contributes to tongue overgrowth comes from mice lacking p57Kip2 and carrying an H19 deletion, in which the tongue was enlarged [53]. Knockdown of CDKN1C with siRNA in satellite cells from donors without BWS did not increase EdU incorporation, despite efficient knockdown shown by RT-qPCR, and we report this as a negative result. It does not exclude a role for CDKN1C, for three reasons. The cells were proliferating, a state in which CDKN1C is already below reliable detection (Fig. 3a), so little remained to remove. p57Kip2 and p21 act redundantly at cell-cycle exit in myogenic differentiation, so loss of one can be compensated by the other [51], whereas indirubin-3'-monoxime inhibits cyclin E–CDK2, the target they share, as well as other CDKs and GSK-3β. Finally, transient suppression with siRNA may not have been sufficient for a phenotypic effect. While these data show that reduced CDKN1C accompanies the phenotype, they do not demonstrate causality. The enrichment of

CDK4/CDK6 pathways in IC2 LOM satellite cells [20] and our observation that indirubin-3'-monoxime, which inhibits several CDKs and GSK-3β, reduces proliferation of BWS satellite cells (Fig. 5) are supportive of CDK activity as a target, independently of whether CDKN1C itself is reduced. Because indirubin-3'-monoxime is not specific for individual CDKs, our data do not show which kinase is responsible; inhibition of GSK-3β alone stimulates myogenic differentiation [54], so part of the reduction in EdU incorporation could reflect earlier differentiation rather than cell-cycle arrest. A comparison of selective CDK2, CDK4/6 and GSK-3β inhibitors in the same cells would address this.

Molecular subtype and tissue mosaicism. Macroglossia is a cardinal feature of BWS [2] but its frequency differs by molecular subtype, being less common in pUPD11 than in IC2 LOM or IC1 gain of methylation [18]. Severity also differs: macroglossia severe enough to need reduction surgery is most frequent in IC2 LOM, followed by pUPD11, and is rarely needed in IC1 gain of methylation [55]. IC2 LOM and pUPD11 both reduce maternal CDKN1C expression, whereas IC1 gain of methylation acts mainly through the IGF2/H19 domain, so a CDKN1C-based mechanism would be expected to apply mainly to IC2 LOM and pUPD11. Tichy et al. [6, 20] further propose that the two subtypes reach the same phenotype by different routes: a cell-intrinsic hypertrophic program in IC2 LOM and, in pUPD11, a progenitor state that depends on signals from fibro-adipogenic progenitors. Because BWS is often mosaic and the epigenotype can differ between blood and tongue [56, 57], the subtype assigned from blood may not reflect the tongue. Children who undergo tongue reduction also have higher levels of blood mosaicism than those who do not [58]. Only one of our patients (7 months, IC2 LOM) has a molecular diagnosis from clinical testing. For the multiome donor, the higher KvDMR1 accessibility fits either IC2 LOM or pUPD11, and our data do not distinguish between them; methylation and SNP-array testing would be needed to assign the subtype and to assess IC1. This region is relevant to the myogenic program: MYOD induces CDKN1C by binding a distal element within KvDMR1 and modifying higher-order chromatin structure at the locus [59]. Altered chromatin at KvDMR1 could therefore uncouple CDKN1C from MYOD-driven cell-cycle exit, which would fit the combination of more MYOD1/MYOG accessibility, more Ki67 + nuclei in tissue and more cell-cycle gene expression in the multiome that we observed. This remains a hypothesis. Because imprinting control region methylation is established in the germline and maintained through life, and both datasets measure chromatin, this comparison is less affected by the age and nuclei-versus-cells differences that limit our gene expression comparisons. With one donor and three adult libraries, however, it is an observation rather than a test. Methylation testing of the resected tongue would allow our results to be interpreted by subtype, as was done for liver tissue in a single-nucleus multiome study of BWS [60].

The satellite cell niche. Satellite cell quiescence and activation are controlled not only by cell-intrinsic programs but also by the niche: growth factors and cytokines from neighbouring cells, the extracellular matrix, and immune signals [61]. Fibro-adipogenic progenitors (FAPs) are a major source of these signals and promote myogenesis after injury [62, 63]. In BWS tongue, PDGFRA+ FAPs are not expanded, collagen deposition is not increased, and BWS FAPs do not proliferate more than control FAPs [6]. Conditioned medium from pUPD11 FAPs, but not from IC2 LOM or control FAPs, nonetheless increased MYOGENIN expression and fusion of normal human myoblasts without changing their proliferation, an

effect linked to secreted cathepsin L and transferrin [6]. Such signals act on differentiation and fusion rather than proliferation, so they would add to, rather than explain, the larger number of Ki67 + nuclei we observed. We therefore asked whether an altered niche could contribute to the satellite cell phenotype, for example by abnormal paracrine signals that push satellite cells out of quiescence and toward differentiation. We did not isolate FAPs, but our satellite-cell sort carried over a small number of fibroblast-like (COL1A1 + or PDGFRA+) nuclei. These contaminating nuclei are few, were profiled by RNA only and were not validated as FAPs. They did not express more TF or CTSL than adult fibroblast-like cells. In myogenic nuclei, after correction for gene length, which biases single-nucleus detection, the transferrin receptor TFRC and the receptors for the other FAP-derived ligands were within the adult range at both the RNA and promoter-accessibility levels, as were gene-set scores for iron uptake and response, lysosomal and autophagy genes, and TGF-beta targets. By contrast, a differentiation and fusion program (MYOG, MYMX, CDH15, CAV3) was above every adult donor at both the RNA and promoter levels. This is the endpoint that pUPD11 FAP medium enhanced [6], but nothing on the transferrin or cathepsin L axis was raised in our donor that could explain it, which favours a satellite-cell-intrinsic mechanism. These observations come from one donor whose subtype was not tested clinically and measure RNA rather than secreted protein. If the donor has IC2 LOM, the subtype in which Tichy et al. found no FAP effect, they are what that model predicts, and niche effects remain possible in pUPD11. The niche and a cell-intrinsic 11p15 effect are not mutually exclusive. The increased KvDMR1 accessibility was measured in purified satellite cells and so reflects the satellite cells themselves, while niche signals could amplify their activation in the tissue. One route by which such signals could act is the Hippo–YAP pathway, which regulates proliferation [64] and self-renewal [65, 66] of mouse satellite cells (reviewed in [61]); we did not measure YAP activity, and YAP1 RNA in the BWS satellite cells showed no CDKN1C-like deficit, so whether this pathway contributes remains open.

IGF receptors in BWS satellite cells. Two receptors of the IGF axis stood out in the BWS satellite-cell nuclei after correction for gene length. IGF2R was detected in 33.5% of myogenic nuclei compared with 3.9 to 6.9% in adult donors, and its promoter was more accessible than in all three adult scATAC libraries. IGF1R was also higher at both the RNA and promoter levels. IGF2R, the cation-independent mannose-6-phosphate receptor, takes up mannose-6-phosphate-tagged lysosomal enzymes, including procathepsin L, and binds IGF2 and targets it for lysosomal degradation without transmitting a mitogenic signal. Loss of Igf2r in mice causes fetal overgrowth through excess IGF2 [67, 68], and IGF2R pathway dysfunction has been reported in BWS cell lines [10]. We therefore hypothesize that higher IGF2R in BWS satellite cells reflects a compensatory response to increased IGF2 exposure, with IGF1R carrying the growth signal. This hypothesis comes from a single donor. We did not measure IGF2 itself, and the expression of IGF2, IGF2R and IGF1R needs to be confirmed in tissue.

Tongue compared with other muscles. Tongue satellite cells arise from occipital somites and differ in lineage and gene expression from limb satellite cells [69, 70]. Mouse tongue regenerates with similar or slightly faster kinetics than tibialis anterior, and tongue satellite cells retain distinct HOX-gene positional identity in culture [71]. Our healthy reference data come from adult limb and trunk muscle, so some differences between BWS tongue and these controls may reflect muscle of origin rather than BWS.

Age at surgery. Four of the six BWS tongues were reduced before one year of age, consistent with current practice of operating early, before macroglossia interferes with feeding, airway and speech [2, 72]. The higher Ki67 and EdU fractions reported here were therefore measured mainly in infant tissue, whereas the matched-state CDKN1C result comes from an 8-year-old donor; this series cannot establish when during development these differences arise. BWS arises from several distinct molecular lesions (IC2 LOM, pUPD11, IC1 gain of methylation and CDKN1C variants) that differ in phenotype and in the severity of macroglossia [2, 18, 55], may act on the tongue through different cellular routes [6, 20], and are often mosaic, with a tongue epigenotype that can differ from that in blood [56, 57]. Any future approach directed at satellite cells would therefore likely need to be matched to the molecular subtype, and our series is too small to show pathway differences between subtypes or individual patients.

Limitations. This study has several limitations. Age-matched tongue from children without BWS or macroglossia was not available to us. Such tissue comes only from children undergoing tongue surgery for another reason or post mortem, as in the autopsy controls of Tichy et al. [20], and post-mortem tissue is not suited to the live-cell sorting, culture and multiome experiments performed here. Our pediatric control was older than the infant BWS patients and had macroglossia of a different cause, and the adult tongue differs from BWS tongue in age as well as diagnosis. The single-cell reference consisted of FACS-purified satellite cells from limb and trunk muscles of 12 healthy adults aged 20 to 87 years, profiled by whole-cell scRNA-seq, whereas the BWS sample was profiled by single-nucleus multiome. Both were purified on the same FACS gate (lineage-negative CXCR4 + CD29+ CD56+), so differences in cell selection are unlikely to explain the comparisons. Age is a particular concern for imprinted genes, because Igf2, H19, Cdkn1c and other members of an imprinted gene network are down-regulated during postnatal growth deceleration in multiple organs [73] and are reactivated in adult muscle only during regeneration [74]. Age therefore cannot simply be subtracted from a comparison of a child with adults. A second problem is technical. Single-nucleus profiling detects long genes such as CDK6, PAX7 and KCNQ1OT1 more readily than whole-cell profiling does, and detects short and immediate-early transcripts such as CDKN1C, FOS and JUNB less readily [75]. For this reason we treated single-gene differences between the BWS satellite cells and the adult cells as observations only, and only when they survived ranking against genes of similar length. KCNQ1OT1 did not. CDK8 survived the length correction but was not supported by chromatin and was never tested functionally, so we do not interpret it. Re-counting the adult data with intronic reads included would reduce this bias. Large single-nucleus multiome atlases of adult human muscle [42] could serve as nucleus-matched references in future work. Cell-state proportions (cycling and MYOG+ cells) are less sensitive to it, and these were compared after matching sequencing depth. The multiome represents a single BWS donor, so comparisons with adults are descriptive and were not tested statistically. FOS was detected in about half of BWS satellite cells. FOS and other immediate-early genes are induced by tissue dissociation and cell isolation [76–78], so they cannot be taken as evidence of activation in vivo. Finally, the number of patients was small and included different molecular subtypes. Unlike inbred mouse strains, human donors differ widely in age, genetic background and muscle of origin, so variation between donors is large and small groups have limited statistical power. For this reason we report the consistency across

donors alongside P values. Identifying PAX7 + cells in situ, at the periphery of myofibers in tissue sections, is the most direct way to be sure that the cells studied are satellite cells: once isolated, satellite cells begin to activate within hours [76–78], human satellite cells purified with the same FACS strategy differ among themselves in how they respond to activation [25], and in culture they become myogenic progenitors. Our conclusions about satellite cells therefore rest on the tissue counts (Fig. 2) and on nuclei isolated immediately after sorting, without culture (multiome), whereas the EdU experiments describe the cultured progeny of sorted satellite cells. Despite these limitations, the observations on which our conclusions rest were consistent across donors: Ki67 + nuclei were more frequent in both BWS tongues than in either control tongue, CDKN1C fell below detection on activation in all six donor-matched pairs, and indirubin-3'-monoxime reduced EdU incorporation in all seven donors.

Future directions. Several experiments would test these interpretations. Restoring CDKN1C expression in BWS satellite cells, or knocking it down in quiescent or differentiating satellite cells from children without BWS, would test whether loss of p57Kip2 contributes to the phenotype. Because p21 can compensate for loss of p57Kip2 [51], knocking down CDKN1C and CDKN1A together in satellite cells from children without BWS would test the hypothesis that losing both brakes reproduces the BWS phenotype. CUT&RUN for MYOD in BWS and control satellite cells would test the hypothesis proposed above that MYOD binds the more accessible KvDMR1 region and contributes to reduced CDKN1C expression. RNAscope for CDKN1C, IGF2 and IGF2R in BWS tongue and in age-appropriate non-BWS tongue would test in tissue the changes suggested here. Co-staining of Ki67 with MYOG or MYOD in tissue sections would show whether the PAX7-negative cycling cells are committed myogenic progenitors. Imaging-based spatial transcriptomics of cryopreserved BWS and control tongue would measure gene expression in PAX7 + cells in their niche, without isolation or culture. Co-culture of activated FAPs with satellite cells from children with BWS and from age-matched children without BWS, followed by EdU and MYOD/MYOG readouts, would separate intrinsic and niche contributions. These experiments are proposals and are outside the scope of the present study.

If confirmed in more patients, these findings would support studying cell-cycle modulation as a treatment approach to macroglossia.

Conclusions

Tongue from children with BWS contained more Ki67 + nuclei than control tongue, and satellite cells from one BWS tongue showed features of activation, with more nuclei expressing cell-cycle genes or MYOG than adult satellite cells. Chromatin at KvDMR1 was more accessible, consistent with the 11p15 imprinting defect, and in the multiome donor CDKN1C was detected less often within matched cell states than in any adult donor. Indirubin-3'-monoxime, a CDK/GSK-3β inhibitor, reduced the proliferation of both BWS and healthy Hu-MuSC. These findings are consistent with altered cell-cycle regulation in BWS satellite cells and need confirmation in a larger cohort.

Abbreviations

BWS
Beckwith-Wiedemann syndrome
CDK
cyclin-dependent kinase
DAPI
4',6-diamidino-2-phenylindole
EdU
5-ethynyl-2'-deoxyuridine
FACS
fluorescence-activated cell sorting
FBS
fetal bovine serum
GEM
Gel Bead-In-Emulsion
GEO
Gene Expression Omnibus
H&E
hematoxylin and eosin
Hu-MuSC
human muscle satellite cells
IC1, IC2
imprinting control regions 1 and 2
IHC
immunohistochemistry
KvDMR1
KCNQ1OT1 differentially methylated region 1
LOM
loss of methylation
MACS
magnetic-activated cell sorting
PBS
phosphate-buffered saline
PFA
paraformaldehyde
pUPD
paternal uniparental disomy
RT-qPCR
reverse transcription quantitative PCR
scATAC-seq
single-cell assay for transposase-accessible chromatin using sequencing

scRNA-seq
single-cell RNA sequencing
SNN
shared nearest neighbor
TSS
transcription start site
UMI
unique molecular identifier
WNN
weighted nearest neighbor

Declarations

Ethics approval and consent to participate

This study was approved by the Institutional Review Board of the University of California, San Francisco (protocol 11-07323). Written informed consent was obtained from all adult participants and from the parents or legal guardians of participants under 18 years of age with assent from age-appropriate subjects.

Consent for publication

Not applicable.

Availability of data and materials

Processed single-nucleus multiome data generated in this study (gene expression count matrices, ATAC fragment files and cell-type and cell-state annotations) have been submitted to the Gene Expression Omnibus (accession number to be provided). Access to the raw sequencing reads is open. The adult satellite-cell scRNA-seq reference data were previously published by our laboratory [25] and are available from Dryad (doi:10.7272/Q65X273X). The close-to-quiescence and activated scATAC libraries of the 56-year-old male were previously published by our laboratory [26], with data and analysis scripts at github.com/kstriedinger/PomerantzLab_ATAC1. The close-to-quiescence scATAC library of the 52-year-old male has not been published before and has been submitted to the Gene Expression Omnibus together with the multiome data (accession number to be provided). Analysis code for this study is provided to the editors and reviewers with the submission; code and other data are available from the corresponding author on request.

Competing interests

The authors declare that they have no competing interests.

Funding

This work was supported by the Caroline Damsky Award of the Program in Craniofacial Biology, University of California San Francisco (fiscal year 2021–2022) to KS and by the National Institute of Arthritis and Musculoskeletal and Skin Diseases of the National Institutes of Health under award number R01AR072638 to JHP. Support from the UCSF Craniofacial Center is also acknowledged. The content is solely the responsibility of the authors and does not necessarily represent the official views of the National Institutes of Health. The funders had no role in the design of the study, the collection, analysis and interpretation of data, or the writing of the manuscript.

Authors' contributions

KS conceived the study, obtained funding (Caroline Damsky Award), designed and performed all experiments, analysed the data and wrote the manuscript. JHP conceived the study, supervised the work, obtained funding (NIH R01AR072638) and edited the manuscript. All authors read and approved the final manuscript.

Acknowledgements

We thank the patients and their families. We thank Emilie Barruet and the residents and surgeons at UCSF for help collecting tissue. We also thank the UCSF Parnassus Flow Cytometry CoLab and the UCSF Genomics CoLab for accommodating our clinical samples.

References

1. Shuman C, Kalish JM, Weksberg R. Beckwith-Wiedemann syndrome. In: Adam MP, et al. editors. GeneReviews®. Seattle (WA). University of Washington, Seattle; 1993–.
2. Brioude F, Kalish JM, Mussa A, Foster AC, Bliek J, Ferrero GB, et al. Expert consensus document: clinical and molecular diagnosis, screening and management of Beckwith-Wiedemann syndrome: an international consensus statement. Nat Rev Endocrinol. 2018;14:229–49.
3. Brzezinski J, Shuman C, Choufani S, Ray P, Stavropoulos DJ, Basran R, et al. Wilms tumour in Beckwith-Wiedemann syndrome and loss of methylation at imprinting centre 2: revisiting tumour surveillance guidelines. Eur J Hum Genet. 2017;25:1031–9.
4. Weksberg R, Nishikawa J, Caluseriu O, Fei YL, Shuman C, Wei C, et al. Tumor development in the Beckwith-Wiedemann syndrome is associated with a variety of constitutional molecular 11p15 alterations including imprinting defects of KCNQ1OT1. Hum Mol Genet. 2001;10:2989–3000.
5. Weksberg R, Shuman C, Smith AC. Beckwith-Wiedemann syndrome. Am J Med Genet C Semin Med Genet. 2005;137C:12–23.
6. Tichy ED, Pawar S, Newsome M, Fallon M, Nguyen AT, Kalish-Schur G, Byrne MA, Kinnear D, Kozakewich H, Kalish JM. Fibroadipogenic progenitor cells contribute to tongue skeletal muscle hypertrophy in Beckwith-Wiedemann syndrome. bioRxiv. 2026. 10.64898/2026.08.18.745577
7. Ainuz BY, Geisler EL, Hallac RR, Perez JK, Seaward JR, Kane AA. Anterior W tongue reduction for macroglossia in Beckwith-Wiedemann syndrome. Cleft Palate Craniofac J. 2022;59:1145–54.

8. Kim DW, Kim JK, Huh G, Lee DY, Kwon SK. Tongue reduction surgery improves mandibular prognathism in Beckwith-Wiedemann syndrome without compromising tongue function. Clin Exp Otorhinolaryngol. 2023;16:67–74.
9. Wagner CS, et al. Associations between the timing of tongue reduction surgery, (epi)genotype, and dentoskeletal development in patients with Beckwith-Wiedemann syndrome. J Craniomaxillofac Surg. 2023;51:568–73.
10. Pileggi S, Colombo EA, Ancona S, Quadri R, Bernardelli C, Colapietro P, et al. Dysfunction in IGF2R pathway and associated perturbations in autophagy and WNT processes in Beckwith-Wiedemann syndrome cell lines. Int J Mol Sci. 2024;25:3586. 10.3390/ijms25073586.
11. Choufani S, Shuman C, Weksberg R. Beckwith-Wiedemann syndrome. Am J Med Genet C Semin Med Genet. 2010;154C:343–54.
12. Choufani S, Shuman C, Weksberg R. Molecular findings in Beckwith-Wiedemann syndrome. Am J Med Genet C Semin Med Genet. 2013;163C:131–40.
13. Liao J, Zeng TB, Pierce N, Tran DA, Singh P, Mann JR, et al. Prenatal correction of IGF2 to rescue the growth phenotypes in mouse models of Beckwith-Wiedemann and Silver-Russell syndromes. Cell Rep. 2021;34:108729.
14. Li M, et al. Imprinting status of 11p15 genes in Beckwith-Wiedemann syndrome patients with CDKN1C mutations. Genomics. 2001;74:370–6.
15. Henry I, Bonaiti-Pellié C, Chehensse V, Beldjord C, Schwartz C, Utermann G, et al. Uniparental paternal disomy in a genetic cancer-predisposing syndrome. Nature. 1991;351:665–7. 10.1038/351665a0.
16. Smith AC, Shuman C, Chitayat D, Steele L, Ray PN, Bourgeois J, et al. Severe presentation of Beckwith-Wiedemann syndrome associated with high levels of constitutional paternal uniparental disomy for chromosome 11p15. Am J Med Genet A. 2007;143A:3010–5.
17. George AM, et al. Expanded phenotype and cancer risk in patients with Beckwith-Wiedemann spectrum caused by CDKN1C variants. Am J Med Genet A. 2024;194:e63777.
18. Mussa A, Russo S, De Crescenzo A, Freschi A, Calzari L, Maitz S, et al. (Epi)genotype-phenotype correlations in Beckwith-Wiedemann syndrome. Eur J Hum Genet. 2016;24:183–90.
19. Oyama Y, et al. Macroglossia in Beckwith-Wiedemann syndrome is attributed to skeletal muscle hyperplasia. Case Rep Dent. 2020;2020:8871961.
20. Tichy ED, Nguyen AT, Byrne MA, Pradieu RD, Kalish-Schur G, Fallon M et al. Myogenic dysregulation underlies tongue overgrowth in Beckwith-Wiedemann syndrome. bioRxiv. 2026. 10.64898/2026.05.18.725925
21. Chargé SB, Rudnicki MA. Cellular and molecular regulation of muscle regeneration. Physiol Rev. 2004;84:209–38.
22. Striedinger K, Barruet E, Pomerantz JH. Purification and preservation of satellite cells from human skeletal muscle. STAR Protoc. 2021;2:100302.

23. Garcia SM, Tamaki S, Xu X, Pomerantz JH. Human satellite cell isolation and xenotransplantation. Methods Mol Biol. 2017;1668:105–23. 10.1007/978-1-4939-7283-8_8.
24. Garcia SM, Tamaki S, Lee S, Wong A, Jose A, Dreux J, et al. High-yield purification, preservation, and serial transplantation of human satellite cells. Stem Cell Rep. 2018;10:1160–74. 10.1016/j.stemcr.2018.01.022.
25. Barruet E, Garcia SM, Striedinger K, Wu J, Lee S, Byrnes L, et al. Functionally heterogeneous human satellite cells identified by single cell RNA sequencing. eLife. 2020;9:e51576.
26. Striedinger K, Barruet E, Atamaniauc E, Linquist K, Knott C, Brack A, Pomerantz JH. Control of quiescence and activation of human muscle stem cells by cytokines. PLoS ONE. 2025;20(12):e0327701. 10.1371/journal.pone.0327701.
27. Mademtzoglou D, Asakura Y, Borok MJ, Alonso-Martin S, Mourikis P, Kodaka Y, et al. Cellular localization of the cell cycle inhibitor Cdkn1c controls growth arrest of adult skeletal muscle stem cells. eLife. 2018;7:e33337.
28. Hoessel R, Leclerc S, Endicott JA, Nobel ME, Lawrie A, Tunnah P, et al. Indirubin, the active constituent of a Chinese antileukaemia medicine, inhibits cyclin-dependent kinases. Nat Cell Biol. 1999;1:60–7.
29. Leclerc S, Garnier M, Hoessel R, Marko D, Bibb JA, Snyder GL, et al. Indirubins inhibit glycogen synthase kinase-3β and CDK5/p25, two protein kinases involved in abnormal tau phosphorylation in Alzheimer's disease. A property common to most cyclin-dependent kinase inhibitors? J Biol Chem. 2001;276:251–60. 10.1074/jbc.M002466200.
30. McFarlane C, Hui GZ, Amanda WZ, Lau HY, Lokireddy S, Xiaojia G, et al. Human myostatin negatively regulates human myoblast growth and differentiation. Am J Physiol Cell Physiol. 2011;301:C195–203. 10.1152/ajpcell.00012.2011.
31. Endesfelder S, Bucher S, Kliche A, Reszka R, Speer A. Transfection of normal primary human skeletal myoblasts with p21 and p57 antisense oligonucleotides to improve their proliferation: a first step towards an alternative molecular therapy approach of Duchenne muscular dystrophy. J Mol Med (Berl). 2003;81:355–62. 10.1007/s00109-003-0439-6.
32. Andresini O, Rossi MN, Matteini F, Petrai S, Santini T, Maione R. The long non-coding RNA Kcnq1ot1 controls maternal p57 expression in muscle cells by promoting H3K27me3 accumulation to an intragenic MyoD-binding region. Epigenetics Chromatin. 2019;12:8. 10.1186/s13072-019-0253-1.
33. Feng X, Naz F, Juan AH, Dell'Orso S, Sartorelli V. Identification of skeletal muscle satellite cells by immunofluorescence with Pax7 and laminin antibodies. J Vis Exp. 2018;13457212. 10.3791/57212.
34. Satpathy AT, Granja JM, Yost KE, Qi Y, Meschi F, McDermott GP, et al. Massively parallel single-cell chromatin landscapes of human immune cell development and intratumoral T cell exhaustion. Nat Biotechnol. 2019;37:925–36.
35. R Core Team. R: a language and environment for statistical computing. Vienna: R Foundation for Statistical Computing; 2022.

36. Hao Y, Hao S, Andersen-Nissen E, Mauck WM 3rd, Zheng S, Butler A, et al. Integrated analysis of multimodal single-cell data. Cell. 2021;184:3573–e8729.
37. Stuart T, Srivastava A, Madad S, Lareau CA, Satija R. Single-cell chromatin state analysis with Signac. Nat Methods. 2021;18:1333–41.
38. Stuart T, Srivastava A, Madad S, Lareau CA, Satija R. Author correction: single-cell chromatin state analysis with Signac. Nat Methods. 2022;19:257.
39. Schep AN, Wu B, Buenrostro JD, Greenleaf WJ. chromVAR: inferring transcription-factor-associated accessibility from single-cell epigenomic data. Nat Methods. 2017;14:975–8. 10.1038/nmeth.4401.
40. 10x Genomics. Nuclei isolation for single cell multiome ATAC + gene expression sequencing. Demonstrated Protocol CG000365 (revision in use in 2020). Pleasanton (CA): 10x Genomics; [cited 2026 Oct 12]. Available from: https://www.10xgenomics.com/support/single-cell-multiome-atac-plus-gene-expression/documentation/steps/sample-prep/nuclei-isolation-for-single-cell-multiome-atac-plus-gene-expression-sequencing
41. Li Y, Li C, Zhou Q, Liu X, Qiao Y, Xie T, et al. Multiomics and cellular senescence profiling of aging human skeletal muscle uncovers Maraviroc as a senotherapeutic approach for sarcopenia. Nat Commun. 2025;16:6207. 10.1038/s41467-025-61403-y.
42. Lai Y, Ramírez-Pardo I, Isern J, An J, Perdiguero E, Serrano AL, et al. Multimodal cell atlas of the ageing human skeletal muscle. Nature. 2024;629:154–64. 10.1038/s41586-024-07348-6.
43. Hafemeister C, Satija R. Normalization and variance stabilization of single-cell RNA-seq data using regularized negative binomial regression. Genome Biol. 2019;20:296. 10.1186/s13059-019-1874-1.
44. De Micheli AJ, Spector JA, Elemento O, Cosgrove BD. A reference single-cell transcriptomic atlas of human skeletal muscle tissue reveals bifurcated muscle stem cell populations. Skelet Muscle. 2020;10:19. 10.1186/s13395-020-00236-3.
45. Naito M, Mori M, Inagawa M, Miyata K, Hashimoto N, Tanaka S, et al. Dnmt3a regulates proliferation of muscle satellite cells via p57Kip2. PLoS Genet. 2016;12:e1006167.
46. Fukada S, Uezumi A, Ikemoto M, Masuda S, Segawa M, Tanimura N, et al. Molecular signature of quiescent satellite cells in adult skeletal muscle. Stem Cells. 2007;25:2448–59.
47. Gattazzo F, Laurent B, Relaix F, Rouard H, Didier N. Distinct phases of postnatal skeletal muscle growth govern the progressive establishment of muscle stem cell quiescence. Stem Cell Rep. 2020;15:597–611.
48. Bachman JF, Klose A, Liu W, Paris ND, Blanc RS, Schmalz M, et al. Prepubertal skeletal muscle growth requires Pax7-expressing satellite cell-derived myonuclear contribution. Development. 2018;145:dev167197. 10.1242/dev.167197.
49. Verdijk LB, Snijders T, Drost M, Delhaas T, Kadi F, van Loon LJC. Satellite cells in human skeletal muscle; from birth to old age. Age (Dordr). 2014;36:545–57.
50. Xi H, Langerman J, Sabri S, Chien P, Young CS, Younesi S, et al. A human skeletal muscle atlas identifies the trajectories of stem and progenitor cells across development and from human pluripotent stem cells. Cell Stem Cell. 2020;27:158–e7610. 10.1016/j.stem.2020.04.017.

51. Zhang P, Wong C, Liu D, Finegold M, Harper JW, Elledge SJ. p21CIP1 and p57KIP2 control muscle differentiation at the myogenin step. Genes Dev. 1999;13:213–24.
52. Reynaud EG, Pelpel K, Guillier M, Leibovitch MP, Leibovitch SA. p57Kip2 stabilizes the MyoD protein by inhibiting cyclin E-Cdk2 kinase activity in growing myoblasts. Mol Cell Biol. 1999;19:7621–9.
53. Caspary T, Cleary MA, Perlman EJ, Zhang P, Elledge SJ, Tilghman SM. Oppositely imprinted genes p57Kip2 and Igf2 interact in a mouse model for Beckwith-Wiedemann syndrome. Genes Dev. 1999;13:3115–24.
54. van der Velden JLJ, Langen RCJ, Kelders MCJM, Wouters EFM, Janssen-Heininger YMW, Schols AMWJ. Inhibition of glycogen synthase kinase-3β activity is sufficient to stimulate myogenic differentiation. Am J Physiol Cell Physiol. 2006;290:C453–62. 10.1152/ajpcell.00068.2005.
55. Romeo DJ, Banala M, Wu M, Ng JJ, Massenburg BB, George AM, et al. A novel macroglossia severity index for Beckwith-Wiedemann syndrome. Ann Surg. 2025;282:1070–5. 10.1097/SLA.0000000000006301.
56. Alders M, et al. Methylation analysis in tongue tissue of BWS patients identifies the (epi)genetic cause in 3 patients with normal methylation levels in blood. Eur J Med Genet. 2014;57:293–7.
57. Duffy KA, Hathaway ER, Klein SD, Ganguly A, Kalish JM. Epigenetic mosaicism and cell burden in Beckwith-Wiedemann syndrome due to loss of methylation at imprinting control region 2. Cold Spring Harb Mol Case Stud. 2021;7:a006115.
58. Romeo DJ, Wagner CS, Massenburg BB, Reddy N, Wu M, Ng JJ, et al. Trends in blood mosaicism and clinical phenotype score in patients with Beckwith-Wiedemann syndrome evaluated for tongue reduction surgery. Plast Reconstr Surg. 2025;155:e573–80. 10.1097/PRS.0000000000011404.
59. Busanello A, Battistelli C, Carbone M, Mostocotto C, Maione R. MyoD regulates p57kip2 expression by interacting with a distant cis-element and modifying a higher order chromatin structure. Nucleic Acids Res. 2012;40:8266–75.
60. Nirgude S, Tichy ED, Liu Z, Kavari SL, Pradieu RD, Byrne M, et al. Single-nucleus multiomic analysis of Beckwith-Wiedemann syndrome liver reveals PPARA signaling enrichment and metabolic dysfunction. Commun Biol. 2025;8:495. 10.1038/s42003-025-07961-9.
61. Trentesaux C, Striedinger K, Pomerantz JH, Klein OD. From gut to glutes: the critical role of niche signals in the maintenance and renewal of adult stem cells. Curr Opin Cell Biol. 2020;63:88–101. 10.1016/j.ceb.2020.01.004.
62. Joe AW, Yi L, Natarajan A, Le Grand F, So L, Wang J, et al. Muscle injury activates resident fibro/adipogenic progenitors that facilitate myogenesis. Nat Cell Biol. 2010;12:153–63.
63. Uezumi A, Fukada S, Yamamoto N, Takeda S, Tsuchida K. Mesenchymal progenitors distinct from satellite cells contribute to ectopic fat cell formation in skeletal muscle. Nat Cell Biol. 2010;12:143–52.
64. Judson RN, Tremblay AM, Knopp P, White RB, Urcia R, De Bari C, Zammit PS, Camargo FD, Wackerhage H. The Hippo pathway member Yap plays a key role in influencing fate decisions in muscle satellite cells. J Cell Sci. 2012;125:6009–19.

65. Li L, Fan CM. A CREB-MPP7-AMOT regulatory axis controls muscle stem cell expansion and self-renewal competence. Cell Rep. 2017;21:1253–66. 10.1016/j.celrep.2017.10.031.
66. Sun C, De Mello V, Mohamed A, Ortuste Quiroga HP, Garcia-Munoz A, Al Bloshi A, et al. Common and distinctive functions of the Hippo effectors Taz and Yap in skeletal muscle stem cell function. Stem Cells. 2017;35:1958–72.
67. Lau MM, Stewart CE, Liu Z, Bhatt H, Rotwein P, Stewart CL. Loss of the imprinted IGF2/cation-independent mannose 6-phosphate receptor results in fetal overgrowth and perinatal lethality. Genes Dev. 1994;8:2953–63.
68. Wang ZQ, Fung MR, Barlow DP, Wagner EF. Regulation of embryonic growth and lysosomal targeting by the imprinted Igf2/Mpr gene. Nature. 1994;372:464–7.
69. Harel I, Nathan E, Tirosh-Finkel L, Zigdon H, Guimarães-Camboa N, Evans SM, et al. Distinct origins and genetic programs of head muscle satellite cells. Dev Cell. 2009;16:822–32.
70. Randolph ME, Pavlath GK. A muscle stem cell for every muscle: variability of satellite cell biology among different muscle groups. Front Aging Neurosci. 2015;7:190.
71. Goto A, et al. Tongue muscle for the analysis of head muscle regeneration dynamics. J Dent Res. 2022;101:962–71.
72. Wagner CS, Pontell ME, Salinero LK, Barrero CE, Drust WA, DeMarchis M, et al. (Epi)genotype and timing of tongue reduction predict safety and long-term outcomes in Beckwith-Wiedemann syndrome. Plast Reconstr Surg. 2024;154:1269–77. 10.1097/PRS.0000000000011112.
73. Lui JC, Finkielstain GP, Barnes KM, Baron J. An imprinted gene network that controls mammalian somatic growth is down-regulated during postnatal growth deceleration in multiple organs. Am J Physiol Regul Integr Comp Physiol. 2008;295:R189–96.
74. Martinet C, Monnier P, Louault Y, Benard M, Gabory A, Dandolo L. H19 controls reactivation of the imprinted gene network during muscle regeneration. Development. 2016;143:962–71.
75. Tortelote GG, Pavan RR, Diniz F, El-Dahr S. Gene length is a pivotal feature to explain disparities in transcript capture between single transcriptome techniques. Front Bioinform. 2023;3:1144266. 10.3389/fbinf.2023.1144266.
76. Machado L, Esteves de Lima J, Fabre O, Proux C, Legendre R, Szegedi A, et al. In situ fixation redefines quiescence and early activation of skeletal muscle stem cells. Cell Rep. 2017;21:1982–93.
77. van den Brink SC, Sage F, Vértesy Á, Spanjaard B, Peterson-Maduro J, Baron CS, et al. Single-cell sequencing reveals dissociation-induced gene expression in tissue subpopulations. Nat Methods. 2017;14:935–6.
78. Machado L, Geara P, Camps J, Dos Santos M, Teixeira-Clerc F, Van Herck J, et al. Tissue damage induces a conserved stress response that initiates quiescent muscle stem cell activation. Cell Stem Cell. 2021;28:1125–e357. 10.1016/j.stem.2021.01.017.

Figures

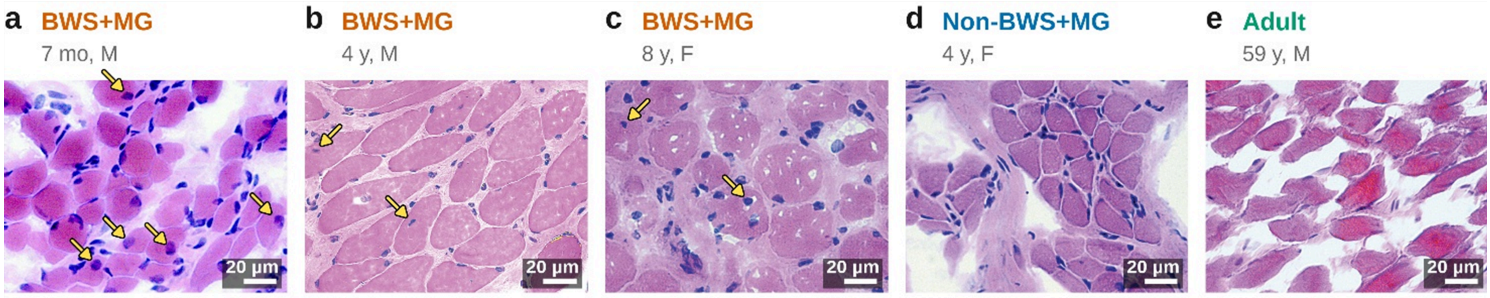

Figure 1

Abnormal histology in macroglossia. H&E-stained tongue sections from children with BWS and macroglossia aged (a) 7 months (male), (b) 4 years (male) and (c) 8 years (female), (d) a 4-year-old female with macroglossia without BWS, and (e) an adult tongue (59-year-old male). BWS tongues show densely packed myofibers of variable size and centrally located nuclei (yellow arrows in a–c; none were seen in d or e). Scale bars, 20 μm (a–e).

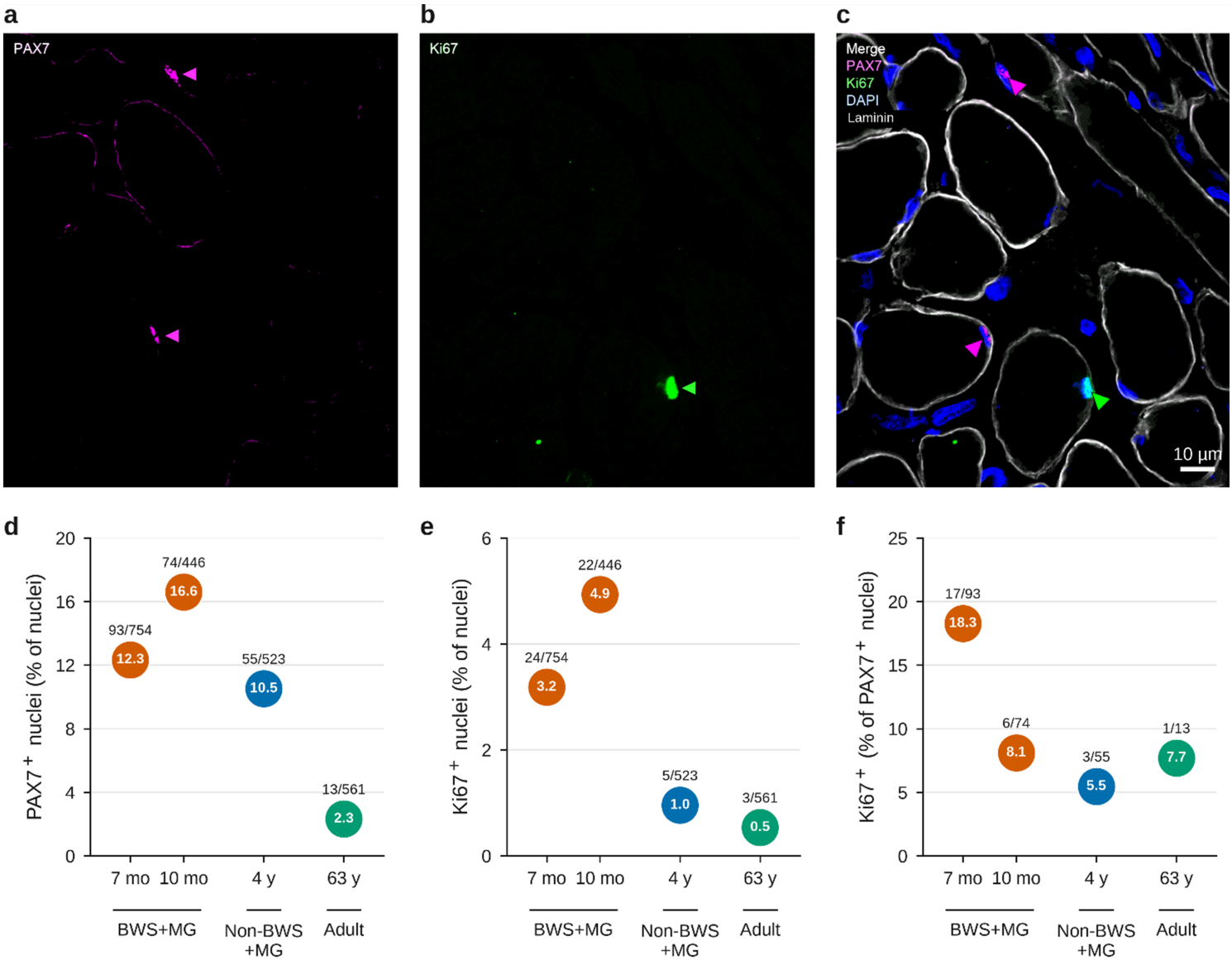

Figure 2

PAX7+ and Ki67+ cells in BWS and control tongue. (a–c) Immunofluorescence for PAX7 (a, magenta), Ki67 (b, green) and merged image (c) with DAPI (blue) and laminin (white) in BWS tongue from a 10-month-old female, one of the tongues counted in d–f; arrowheads mark the same cells in each panel: magenta, two PAX7+ satellite cells (a, c); green, a Ki67+ nucleus (b, c). Images acquired with a 63× objective (Zeiss). (d–f) Percentage of nuclei that are PAX7+ (d), percentage of nuclei that are Ki67+ (e), and percentage of PAX7+ cells that are Ki67+ (f), in BWS macroglossia (BWS + MG; 7 mo and 10 mo), macroglossia without BWS (Non-BWS + MG; 4 y) and adult tongue (63 y). Each circle is one tongue, with counts pooled across 13 to 35 fields (446 to 754 nuclei per tongue). Numbers inside circles, percentage; above each circle, positive / total counted (n/N; all nuclei in d and e, PAX7+ cells in f). No statistical test was applied because each group contained one or two tongues. Scale bar, 10 µm (c).

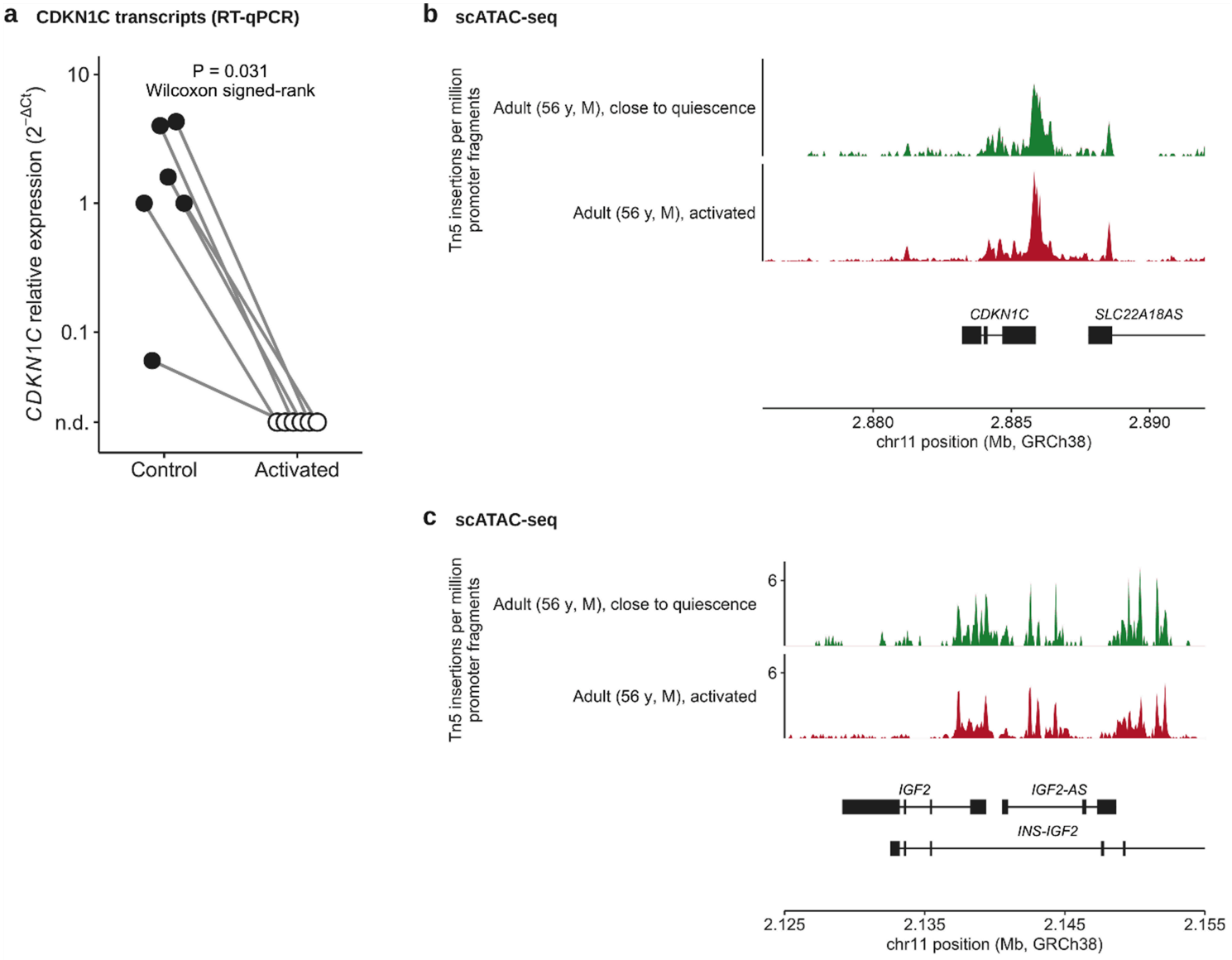

Figure 3

Loss of CDKN1C transcripts upon ex vivo activation of healthy Hu-MuSC. (a) CDKN1C transcripts measured by RT-qPCR (relative expression, 2^−ΔCt, normalized to the reference gene) in quiescent (control) and activated Hu-MuSC from six healthy donors. Samples are donor-matched; lines join samples from the same donor, and values below detection are marked n.d. CDKN1C fell below reliable detection in all six activated samples, and the decrease was consistent when normalized to either ACTB or GAPDH (exact two-sided Wilcoxon signed-rank test, P = 0.031, n = 6 donor-matched pairs). (b, c) Chromatin accessibility (scATAC-seq) at CDKN1C (b) and IGF2 (c) in close-to-quiescence (freshly purified; dark green) and activated (red) Hu-MuSC from the same healthy 56-year-old male donor, shown as Tn5 insertions per million promoter fragments on GRCh38 (hg38), with positions in Mb on chr11; gene models are shown in dark grey.

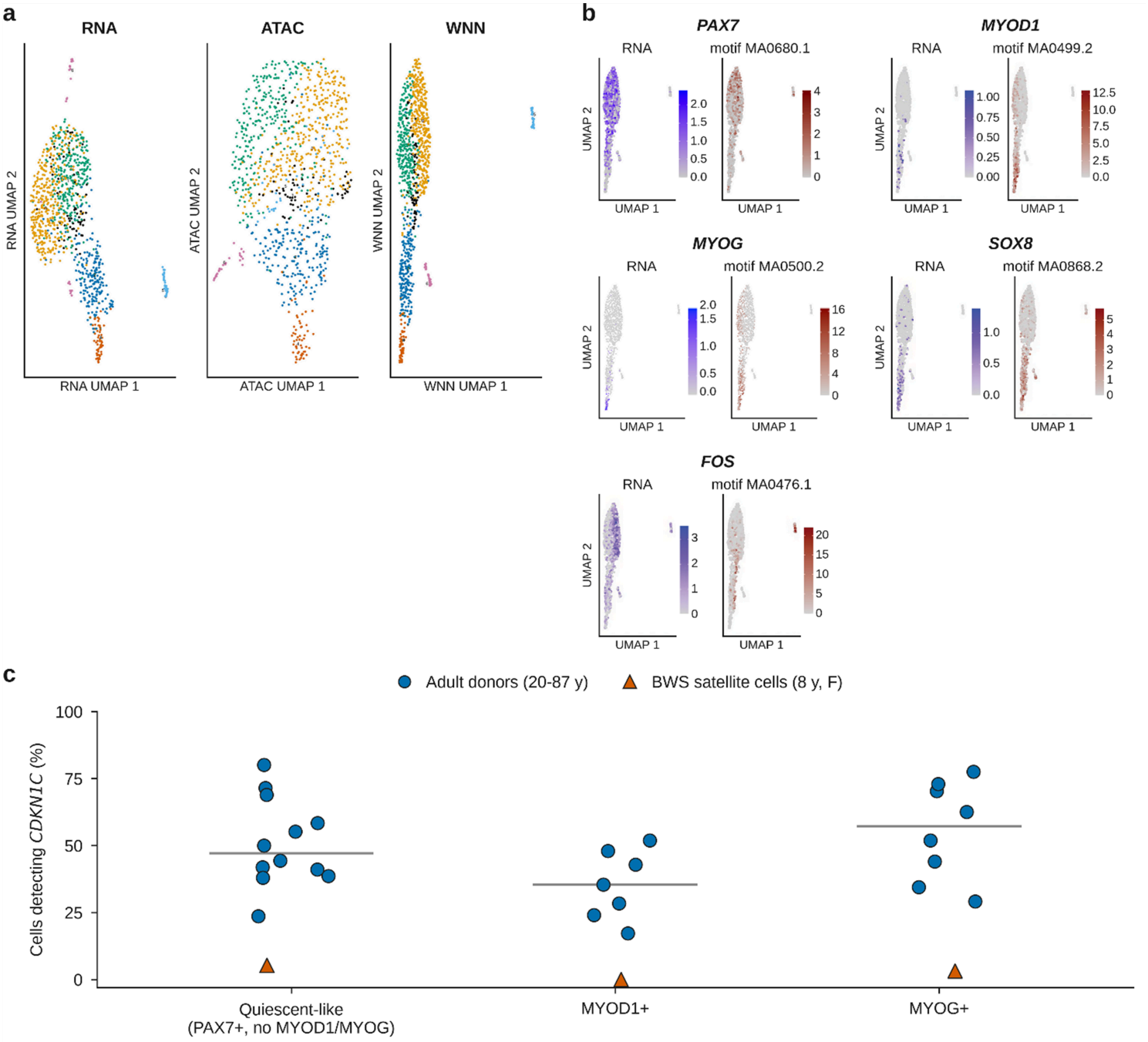

Figure 4

Multiomic data from BWS satellite cells of an 8-year-old female patient with macroglossia. Clustering can be seen in the UMAP representations based on gene expression, ATAC-seq, or weighted-nearest neighbor (WNN) analysis (**a**). The WNN projections show RNA expression of each gene beside chromVAR motif activity for its motif (b; JASPAR IDs in the panel): the myogenic genes PAX7, a marker of Hu-MuSC, MYOD1, MYOG, a marker of differentiation, and SOX8, followed by FOS (FOS is also induced by tissue dissociation). (c) Percentage of myogenic nuclei in which CDKN1C is detected (after downsampling to 1,000 UMIs), by cell state (quiescent-like, PAX7+ MYOD1− MYOG−; MYOD1+; MYOG+), in BWS satellite cells (one donor, 8 years, female; single-nucleus) and in satellite cells from 12 adult donors (20–87 years; single-cell). Circles, individual adult donors (single-cell); triangles, the single BWS donor (single-nucleus); lines, adult median. BWS nuclei and adult donors with cells in each state: quiescent-like, 490 nuclei and 12 donors; MYOD1+, 26 nuclei and 7 donors; MYOG+, 62 nuclei and 8 donors. Descriptive; one BWS donor, no statistical test.

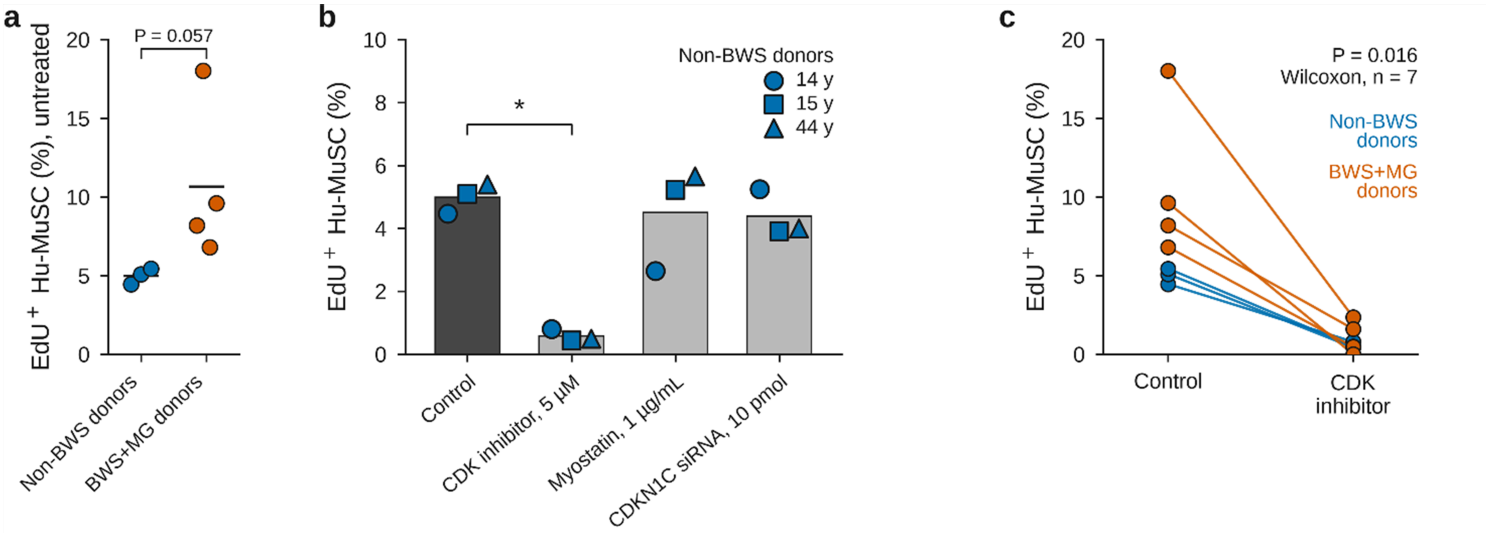

Figure 5

Proliferation of BWS and non-BWS Hu-MuSC at baseline and with a CDK inhibitor. (a) Percentage of EdU+ Hu-MuSC under control conditions in cells from three non-BWS donors (14, 15 and 44 years) and four BWS donors (BWS+MG in the panels, BWS macroglossia; 4 years, 10 months, 7 months and 9 months); the line marks the mean. Exact two-sided Mann–Whitney test, P = 0.057. (b) Percentage of EdU+ Hu-MuSC from the three non-BWS donors (14, 15 and 44 years) under control conditions or after treatment with the CDK/GSK-3β inhibitor indirubin-3'-monoxime (5 µM; "CDK inhibitor" in the panels), recombinant human myostatin (1 µg/mL) or siRNA against CDKN1C (10 pmol); bars, means of n = 3 donors; points, individual donors (circle, 14 years; square, 15 years; triangle, 44 years); * P = 0.007, two-sided paired t-test, control vs CDK inhibitor; myostatin and siRNA, P > 0.4. Myostatin (2 µg/mL) and CDKN1C siRNA (40 pmol) were each quantified in one donor and are not shown. (c) Percentage of EdU+ Hu-MuSC with and without CDK inhibitor in each of the seven donors: non-BWS donors aged 14, 15 and

44 years and BWS donors aged 7 months, 9 months, 10 months and 4 years (the 9-month-old donor had 0% EdU+ cells with the inhibitor); lines join each donor's control and inhibitor values; P = 0.016 (exact two-sided Wilcoxon signed-rank test, n = 7).

Supplementary Files

This is a list of supplementary files associated with this preprint. Click to download.

- Additionalfile3.tif
- Additionalfile2.tif
- Additionalfile4.tif
- Additionalfile1.tif